Cdc42 Partitioning by Chaperone Ydj1 During Asymmetric Division and Aging in Yeast

Pil Jung Kang[1], Hana Mazak[1], Sung Sik Lee[2,3], and Hay-Oak Park[1]*

[1]Department of Molecular Genetics, The Ohio State University, Columbus, OH 43210, USA
[2]Scientific Center of Optical and Electron Microscopy, Institute of Biochemistry, ETH Zurich, Zurich, Switzerland
[3]Institute of Biochemistry, Department of Biology, ETH Zurich, Zurich, Switzerland

*Corresponding author: Department of Molecular Genetics, The Ohio State University, 484 West 12th Ave, Columbus, OH 43210-1292, E-mail: park.294@osu.edu, Tel: 614-688-4575, Fax: 614-292-4466

Running Title: Ydj1-mediated asymmetric distribution of Cdc42 GTPase

Key words: cell asymmetry and polarity, *Saccharomyces cerevisiae*, replicative lifespan, microfluidics-assisted imaging.

Abbreviations: extrachromosomal rDNA circles (ERCs), plasma membrane (PM), endoplasmic reticulum (ER), wild type (WT)

ABSTRACT

The small GTPase Cdc42 is a central regulator of cell polarity, but it is often hyperactivated in aged cells, contributing to senescence and aging in both yeast and animal cells. Yet, the mechanisms underlying its age-related upregulation remain poorly understood. Here, we examine how Cdc42 levels change over successive divisions in budding yeast, which undergoes asymmetric cell division, leading to aging predominantly in mother cells. Using microfluidics-based live-cell imaging and genetic analyses, we find that Cdc42 protein is unevenly distributed between mother and daughter cells during division. Notably, daughter cells inherit lower levels of Cdc42, which helps them rejuvenate. This asymmetry depends on Cdc42's association with endomembranes and requires the presence of farnesylated Ydj1, an Hsp40/DnaJ chaperone tethered to the endoplasmic reticulum. Furthermore, maintaining proper Cdc42 levels relies on its interaction with Ydj1. These findings reveal a chaperone-mediated mechanism that controls Cdc42 partitioning during asymmetric division, linking it to cellular aging—a process that may be conserved in other asymmetrically dividing cells.

INTRODUCTION

Cell polarity is fundamental to various processes, including cell division, migration, and tissue organization. Cdc42 plays a critical role in establishing cell polarity by regulating cytoskeletal organization and directional growth across a wide range of organisms, from yeast to humans [1, 2]. Notably, Cdc42 activity is elevated in aged cells and tissues, such as yeast and hematopoietic stem cells, and its upregulation correlates with a loss of polarity and increased symmetric division [3-7]. Previous studies have shown that heightened Cdc42 activity shortens lifespan in yeast and animals [4, 8-10], yet the mechanisms linking Cdc42 to cellular aging remain unclear.

The replicative lifespan (hereafter, **lifespan**) of budding yeast is defined by the number of cell divisions a mother cell undergoes before senescence [11]. The number of senescent cells increases with aging in multicellular organisms [12], while senescence is likely directly linked to lifespan in yeast. Various cellular features associated with yeast aging are confined to mother cells, and these are also involved in metazoan aging [13, 14]. These features include the increased accumulation of protein aggregates [15-17], silencing loss at the rDNA locus, associated with formation of extrachromosomal rDNA circles (**ERCs**) [18, 19], and defects in mitochondrial integrity [20]. Sir2 silences the rDNA locus and suppresses ERC formation in yeast [21], whereas Fob1 promotes the production of ERCs by decreasing rDNA stability [22]. Accordingly, deletion of *SIR2* shortens lifespan, while deletion of *FOB1* extends lifespan relative to wild type (**WT**) [21, 23].

During polarized growth of budding yeast, the 'polarisome', a multi-protein complex crucial for establishing and maintaining cell polarity [24], facilitates retrograde transport of protein aggregates from daughter to mother cells along actin cables [25]. This process also requires Sir2, which promotes proper folding of actin through the chaperonin CCT [25]. However, in some studies, mutations in the

polarisome components do not completely abolish asymmetric segregation of protein aggregates [26, 27], suggesting that additional mechanisms contribute to mother-cell-specific aging.

Cells that lack Cdc42-inhibitory polarity cues or Rga1, a GTPase-activating protein (GAP) for Cdc42, exhibit shorter lifespans [7, 28]. Microfluidic imaging with a Cdc42-GTP biosensor reveals that Cdc42 is frequently hyperactivated during yeast aging. Interestingly, mild overexpression of Cdc42 results in a shortened lifespan with characteristics of premature aging, despite causing no growth defects during the exponential growth phase [7]. Notably, *rga1Δ* cells, which have elevated Cdc42-GTP levels even at young ages, show further increases in Cdc42-GTP levels as they age. Additionally, individual cells of a *CDC42* overexpressing strain (*CDC42*$_{OV}$), which show mild overexpression evenly in early generations, display a wide range of Cdc42 level increases during aging. These observations led us to investigate how Cdc42 protein levels are regulated throughout the aging process.

Here, we report that Cdc42 levels increase during aging and that Cdc42 is asymmetrically distributed between mother and daughter cells during division. This asymmetric distribution and the maintenance of proper Cdc42 levels depend on its association with endomembranes and its interaction with farnesylated Ydj1, a member of the Hsp40/DnaJ chaperone family. Our findings suggest that Ydj1 promotes retention of Cdc42 in mother cells via **ER** (endoplasmic reticulum) anchoring, thereby aiding daughter cell rejuvenation through low Cdc42 inheritance.

RESULTS AND DISCUSSION

Cdc42 levels increase in old cells, likely limiting lifespan

Given the frequent hyperactivation of Cdc42 in *rga1Δ* cells during aging [7], we asked how Cdc42 protein levels evolve during successive divisions and how daughter cells maintain low Cdc42 levels, despite the strong polarization of Cdc42 to the bud tip early in the cell cycle [29]. We first performed time-lapse imaging of cells expressing Cdc42-mCherry^{SW}, a functional internal fusion [30], and Cdc3-GFP marking the mother and bud compartments. As expected, the mean fluorescence intensity of Cdc42-mCherry^{SW} was highest in small buds early in the cell cycle, then declined as the bud enlarged, reaching a minimum in large buds or newborn daughter cells (Fig. S1). For subsequent analyses, we therefore focused on late M phase or cytokinesis, when Cdc42 is no longer polarized to the bud tip or a new bud site.

To compare Cdc42 levels at different ages at the single-cell level, we performed microfluidic imaging of WT cells expressing Cdc42-mCherry^{SW} (Fig. 1A; Video 1). We measured the mean fluorescence intensity in individual cells during the first three divisions (young age) and the last three divisions before death (old age). These analyses showed that Cdc42 levels increase with age (Fig. 1B). We next tested how reducing Cdc42 protein levels affects lifespan using a hypomorphic *cdc42* mutant (*cdc42-108*$^{R147A\ E148A\ K150A}$), which has approximately 50% lower Cdc42 protein levels than its isogenic WT counterpart (Figs. 1C & S2) but appears phenotypically indistinguishable from WT during exponential growth [31]. Microfluidics-based lifespan assays revealed that *cdc42-108* cells live about 23.5% longer than WT (Fig. 1D). The opposite phenotypes of this hypomorphic *cdc42* mutant and

CDC42OV, which has a reduced lifespan [7], suggest that increased Cdc42 likely plays a causal role in aging.

Upregulation of Cdc42 likely limits lifespan independently of rDNA silencing loss

While Cdc42 functions primarily at the cell cortex to establish polarity, it also localizes to the cytoplasmic face of the nuclear envelope and sites of ER fission [30, 32]. Given that ERCs associate with the nuclear pore complex and accumulate asymmetrically in mother cells [33, 34], we explored whether upregulation of Cdc42 might promote aging by disrupting rDNA silencing. Previous studies have linked distinct terminal bud morphologies to specific aging defects: elongated buds are correlated with loss of rDNA silencing and nucleolar destabilization [35, 36], while round buds are associated with mitochondrial dysfunction [37, 38]. Notably, about 20% of WT cells near death exhibit elongated buds, but this phenotype increases to approximately 60% in a *sir2Δ* mutant [39, 40], suggesting a relationship between silencing loss and elongated bud morphology.

Using microfluidic imaging, we found that aging WT cells in two genetic backgrounds predominantly displayed round buds, with dying cells typically showing no buds or round buds, while elongated buds were rare (Fig. 2A). Similarly, *CDC42ov* cells also infrequently displayed elongated buds. These observations suggest that the elevation of Cdc42 does not induce rDNA silencing loss. To directly test whether Cdc42 promotes aging independently of rDNA silencing loss, we examined the effects of the *cdc42-108* mutation in a *fob1Δ* strain, a long-lived mutant with reduced ERC formation [23]. Remarkably, the *cdc42-108 fob1Δ* double mutant exhibited a lifespan increase of about 21% compared to a *fob1Δ* mutant (Fig. 2B). These findings support the conclusion that Cdc42 upregulation limits lifespan via a mechanism that is independent of rDNA silencing loss.

Cdc42 is asymmetrically distributed during division via its endomembrane association, promoting daughter cell rejuvenation

From microfluidic imaging of the WT cells expressing Cdc42-mCherry^{SW}, we next tracked mean fluorescence intensities in mother and daughter cells across generations. These analyses showed that daughter cells consistently inherited lower levels of Cdc42 than their mothers, regardless of mother's age (Fig. 3A; see Cell 1, Fig. 1A). In rare cases (~19%, n = 42) where daughter cells inherited similarly high Cdc42 levels as their mothers, both cells typically died soon after division (Fig. 3B). These "non-rejuvenating" daughter cells often had cell sizes comparable to their mothers at the final division (e.g., Cell 2 at t = 14:20, Fig. 1A). These observations suggest that Cdc42 becomes enriched in mother cells during asymmetric cell division and that this asymmetric partitioning contributes to daughter cell rejuvenation.

To investigate the basis of Cdc42 asymmetry, we considered two possibilities: (1) retrograde transport of Cdc42 from a bud to its mother, as suggested for segregation of protein aggregates [25]; and (2) differential turnover due to age-related functional decline of the proteasome system. However, retrograde transport occurs mainly during apical growth when Cdc42 and the polarisome remain polarized at the bud tip [41], coinciding with high bud-localized Cdc42 (see Fig. S1). While changes in the proteasome during aging may influence Cdc42 levels, there is little evidence for differential turnover

between young mothers and their daughters. Thus, neither mechanism may adequately explain the Cdc42 asymmetry during division.

Given the Cdc42's localization to the plasma membrane (**PM**) and endomembranes [29, 30, 32], we next asked whether specific membrane associations contribute to Cdc42 partitioning. We tested *cdc42-ritC*, in which the C-terminal CaaX motif is replaced with the hydrophobic tail of mammalian Rit, restricting Cdc42 exclusively to the PM [42]. Although Cdc42-ritC-GFP is less dynamic than WT and exhibits occasionally at more than one bud simultaneously, it still supports polarized growth [42, 43]. Interestingly, Cdc42-ritC-GFP failed to partition asymmetrically between the mother and bud compartments during division (Fig. 3C), suggesting that Cdc42's association with internal membranes is necessary for its asymmetric distribution.

Farnesylated Ydj1 mediates Cdc42 asymmetry and stability

Given the requirement of endomembrane association in Cdc42 partitioning, we tested whether Ydj1—a farnesylated Hsp40 tethered to the ER [44, 45]—is involved in the process. Ydj1 is enriched in mother cells via an ER diffusion barrier and helps retain protein aggregate formation in aging cells [17]. Because a *ydj1Δ* mutant is temperature-sensitive (sick at 30°C and inviable at 37°C) [44, 46], we analyzed Cdc42-mCherry^{SW} localization at 27°C, a semi-permissive temperature (see Fig. S3). While Cdc42 polarized normally in *ydj1Δ* cells in early cell cycle stages, large-budded *ydj1Δ* cells lost Cdc42 asymmetry (Fig. 4, A & B).

Farnesylated Ydj1 diffuses more slowly in mother cells than in their buds [17], raising the possibility that Ydj1 on the ER may contribute to the asymmetric distribution of Cdc42 during division. To assess whether Cdc42 asymmetry depends on farnesylated Ydj1, we examined Cdc42 localization in *ydj1^{C406S}*, a farnesylation-defective mutant [47]. Although Cdc42 asymmetry was partially disrupted in large-budded *ydj1^{C406S}* cells, statistical analyses confirmed a significant association between farnesylated Ydj1 and Cdc42 asymmetry (one-way ANOVA, $p < 0.0001$; Fig. 4B). Additionally, overall Cdc42 protein levels were reduced in *ydj1Δ* and *ydj1^{C406S}* mutants: Cdc42-mCherry^{SW} fluorescence was diminished in both mother and bud compartments of *ydj1* mutant cells (Fig. 4C). Immunoblotting confirmed that total Cdc42 protein was about 2-fold lower in *ydj1Δ* compared to WT (Figs. 4C & S2). Thus, ER-tethered Ydj1 is necessary for both asymmetric distribution and maintaining the proper levels of Cdc42.

Cdc42 physically interacts with Ydj1

We next tested whether Cdc42 physically associates with Ydj1 by a visible immunoprecipitation (VIP) assay [48], which combines immunoprecipitation with fluorescence microscopy. Lysates from cells expressing GFP-Ydj1 and Cdc42-mCherry^{SW} were subjected to pull-down assays using GFP-binding protein (GBP)-conjugated beads [49]. Subsequent fluorescence microscopy revealed that both GFP-Ydj1 and Cdc42-mCherry^{SW} were retained on the beads. In contrast, no signal was detected in a control with untagged Ydj1 (Fig. 4D). These data demonstrate that Cdc42 physically interacts with Ydj1 in vivo.

Our findings indicate that Ydj1 plays a crucial role in maintaining Cdc42 protein homeostasis and mediating its asymmetric partitioning—functions likely contributing to age-related accumulation of Cdc42. Ydj1, along with Hsp70 and Hsp90, is involved in various aspects of protein folding and stability, including the maturation of protein kinases [50, 51]. Notably, farnesylated Ydj1 is necessary for the stability and maturation of Ste11, an Hsp90 client [52]. We suggest that farnesylated Ydj1 may similarly stabilize Cdc42 through its association with the ER. However, prior reports showed elevated Cdc42 levels in *ydj1Δ* cells at 30°C or after shifting to 37°C [53, 54], which contrasts with our observations at 27°C. This discrepancy could be due to temperature-dependent stress responses: *ydj1Δ* mutants exhibit impaired growth and trigger a stress response that increases Hsp70 and Hsp90 levels at 30°C or higher [44, 46, 51]. These heat shock proteins may elevate Cdc42 levels by assisting in its folding or stabilization. Thus, the increase in Cdc42 in *ydj1Δ* mutants at elevated temperatures might result from indirect compensatory mechanisms rather than a direct effect of Ydj1 loss. Further investigation will be required to clarify these effects and distinguish the mechanisms involved under different conditions.

Summary and Limitations

Our study shows that Cdc42 is asymmetrically distributed between mother and daughter cells, influenced by the ER-tethered, farnesylated Ydj1. Notably, Cdc42 levels increase with age, and reducing its levels can extend lifespan. When daughter cells inherit high Cdc42 levels comparable to their mothers, they fail to rejuvenate, suggesting that lower Cdc42 levels may help maintain the replicative potential in daughters. However, it remains unclear whether a specific threshold of Cdc42 determines their proliferative capacity. Ydj1 likely plays a role in stabilizing and retaining Cdc42 in mother cells, contributing to this accumulation. Additionally, it is yet to be determined whether other mechanisms, such as age-associated transcriptional upregulation of *CDC42,* also influence this process.

Although our data suggest that Cdc42 promotes senescence independently of rDNA silencing loss, the mechanisms linking Cdc42 upregulation to aging are not fully understood. Cdc42 is not classified among the "long-lived asymmetrically retained proteins" typically associated with accumulated damage [55]. Many mother cell-enriched proteins, whose depletion extends lifespan, exhibit normal turnover, suggesting that aging or senescence may not be driven solely by damage accumulation [56, 57]. We propose that repeated asymmetric divisions lead to the accumulation of Cdc42 in mother cells, eventually reaching levels that impair cellular function through aberrant signaling, thereby limiting proliferation. While this study raises further questions, it reveals a conserved chaperone-mediated mechanism that links Cdc42 partitioning to replicative aging, which may be relevant to other asymmetrically dividing cells.

MATERIALS AND METHODS

Yeast strains, growth conditions, and plasmids

Standard methods of yeast genetics, DNA manipulation, and growth conditions were used [58]. Yeast strains were grown in rich yeast medium YPD (yeast extract, peptone, dextrose) or the appropriate synthetic medium containing 2% dextrose as a carbon source. All yeast strains used for imaging express

tagged proteins under their native promoters on the chromosomes. For imaging and protein preparation, yeast strains were grown at 27°C, unless indicated otherwise. Low-copy plasmids pRS315-YDJ1, pRS315-ydj1^{C406S} (CEN, *LEU2*), and pRS416-GFP-YDJ1 (CEN, *URA3*) were kind gifts from D. M. Cyr (University of North Carolina) and W. Schmidt (University of Georgia) [47, 59]. Yeast strains used in this study are listed in Supplemental Table S1.

Microscopy and microfluidic imaging

Cells were grown in an appropriate synthetic medium overnight and then freshly subcultured for 3–4 hrs in the same medium. Live-cell imaging, including microfluidics-based imaging, was performed using an inverted microscope (Ti-E; Nikon) fitted with a 100x/1.45 NA Plan-Apochromat Lambda oil immersion objective lens, a 60x/1.4 NA Plan Apochromat Lambda oil immersion objective lens, and DIC optics (Nikon), FITC/GFP, and mCherry/Texas Red filters from Chroma Technology, an Andor iXon Ultra 888 electron-multiplying charge-coupled device (EM CCD) (Andor Technology), Sola Light Engine (Lumencor) solid-state illumination, and the software NIS Elements (Nikon).

Static fluorescence images (Figs. 3 & 4) were captured using a 100x/1.45 NA objective lens (11 z stacks, 0.4 µm step) with cells either mounted on a 2% agarose slab or a glass-bottomed dish (MatTek) containing the indicated medium with 5 µM n-propyl gallate (Sigma), an anti-fade reagent, as previously described [43, 60]. The slab or dish was put directly in a stage top chamber (Okolab) set to 27°C.

Microfluidics setup and growth conditions are essentially the same as previously described [34], except the imaging temperature was maintained at 27°C. Microfluidic devices were fabricated using polydimethylsiloxane (PDMS) by adopting a design [34] that allows simultaneous imaging of multiple strains through independent passages. Microfluidics-assisted time-lapse imaging was performed using an inverted widefield fluorescence microscope (Ti-E; Nikon) equipped with a 60x/1.4 NA objective lens (5 z stacks, 0.5 µm step) and DIC optics (see above). In general, bright-field images were recorded every 15 min throughout the entire experiment, and fluorescence images were captured for the initial 3~4 hrs and a few hours after 12 hrs, 26 hrs, and 50 hrs at multiple XY positions, except indicated. In some cases (Fig. 1A), fluorescence images were captured every 20 min with a minimum exposure throughout the entire experiment.

Image processing and analysis

Images were processed by importing nd2 files using the NIH ImageJ with Bio-Format importer plugin. Mean fluorescence intensities of Cdc42-mCherry^{SW} were quantified by defining a region of interest (ROI) in single-focused z-stack images using the ImageJ oval selection tool only in cells during the late M phase or cytokinesis; i.e., when no polarized Cdc42 signals were detectable at the bud periphery or the incipient bud site (e.g., cells marked with white arrowheads in Fig. 1A). Given that the asymmetric distribution of Cdc42 between mother and bud compartments was established at this cell cycle stage (see Fig. S1), Cdc42 levels at the same cell cycle stage were quantified throughout this study. These values were compared between young and old ages (of the same cell lineages) or between a mother and her daughter by averaging the mean intensity of Cdc42-mCherry^{SW} in the first or last three divisions for young or old cells, respectively (Fig. 1A). Cdc42 levels were similarly quantified and compared in mother-daughter pairs (Figs. 3 & 4B). The global mean intensity of Cdc42-mCherry^{SW} in WT and mutant cells was quantified similarly, except by defining an ROI covering both a mother and its bud

using the ImageJ freehand tool (Fig. 4C). To make figures, fluorescence images were deconvolved by the Iterative Constrained Richardson-Lucy algorithm (NIS Elements) and cropped at selected time points, preferentially at the cell division or soon after division. The same setting of brightness/contrast was applied to adjust images in multiple panels within the same figure.

Determination of lifespan

Lifespan was estimated by counting the number of cell divisions from microfluidic images until cell death or senescence. Cell death was evident morphologically with abruptly shrinking cell size or cell lysis (from DIC images), which was often accompanied by sudden complete loss of fluorescence signals or abrupt appearance of strong autofluorescence in the whole cell. Cells at senescence or near senescence were marked when there was a sudden increase in the cell cycle length (> 5 ~ 6 hrs) with no further division within 8 ~ 12 hrs. Because some daughter cells that were born from very old mothers did not have full lifespan potential, consistent with a previous report [61], those cells that died in less than three cell divisions were excluded from lifespan analyses.

TCA protein extraction and immunoblotting

TCA precipitation was performed by preparing the whole cell extracts from each strain with 10% trichloroacetic acid (TCA), as previously described [62]. Protein precipitates were resuspended in 100 mM Tris (pH 11.0) and 3% SDS, heated to 90°C for 5 min, followed by centrifugation briefly to remove any cell debris. SDS-PAGE was performed on 12.5% polyacrylamide gels, and Western blots were visualized by the LI-COR Odyssey system (LI-COR Biosciences, Lincoln, Nebraska) using the following antibodies: mouse monoclonal anti-Cdc42 antibody (clone 28-10) (EMD Millipore, MABN2485), rabbit polyclonal anti-RFP antibodies (Rockland, 600-401-379), mouse monoclonal anti-alpha tubulin antibody (clone 12G10) (DSHB, University of Iowa) for loading control, and Alexa Fluor^{R} 680 goat anti-rabbit IgG (ThermoFisher Scientific, A32734) or IRDye^{R} 800CW goat anti-mouse IgG (LI-COR Biosciences, 926-32210) secondary antibodies.

Visible Immunoprecipitation (VIP) assay

VIP assays were performed using a total of 80 OD_{600} units of cells from HPY4079 (*CDC42-mCherry^{SW} ydj1*Δ) carrying pRS416-GFP-YDJ1 or pRS315-YDJ1 (as a control), as previously described [60], with the following modifications. Crude cell lysates, prepared with a PBS buffer (1x PBS, pH 7.4, 0.5mM EDTA) containing a cocktail of protease inhibitors (Research Products International) and 0.1 mM PMSF, were centrifuged at 14,000 rpm for 15 min at 4°C to generate the pellet (P10 fraction). Proteins were solubilized from the P10 fraction using 300µl of the extraction buffer (1x PBS, pH 7.4, 200 mM NaCl, 0.5 mM EDTA, 2% Triton) for 1 h at 4°C and subsequently used for pull-down assays with GFP-Trap beads (gta-10, Chromoteck). Following the washing steps, beads, mounted on an agarose slab, were imaged using an inverted microscope TiE with a 40x/ 0.75 Plan Fluor objective lens (Nikon) at room temperature. Static images were captured using DIC optics, FITC/GFP, and mCherry/Texas Red filters (5 z-stacks, 0.5µm step), and single z-slice images were used to make a figure.

Statistical analysis

Data analysis was performed using Prism 10 (GraphPad Software). To determine statistical differences between two sets of cell survival data, the Gehan-Breslow-Wilcoxon test and Log-rank (Mantel-Cox) test were used. For comparison of Cdc42 levels between young and old cells in the same lineage or between mothers and their daughters, paired t-tests were performed to determine statistical significance: ns (not significant) for $p \geq 0.05$; $*p < 0.05$, $***p < 0.001$, and $****p < 0.0001$. Statistical significance of the Cdc42-mCherry^{SW} mean intensity differences between mother-bud pairs among WT and mutant strains was determined by a one-way ANOVA analysis. For comparison of Cdc42-mCherry^{SW} global intensity between WT and mutants, unpaired t-tests were performed. For box graphs, the Tukey method was used to create the whiskers (for minimum and maximum data points), a box with a line (for the upper, lower quartiles, and median), and to mark outliers.

ACKNOWLEDGMENTS
We are grateful to M. Peter and the Department of Biology at ETH Zurich for their generous support with microfluidics and for hosting a short-term visit to the Institute of Biochemistry, ETH Zurich. We also thank K. Kozminski, D. Drubin, W. Schmidt, D. G. Cyr, and S. Martin for yeast strains and plasmids. The authors declare no competing financial interests.

Funding source
This work has been supported in part by a grant from the National Institutes of Health/National Institute on Aging (R21-AG060028), the Ohio State President's Research Excellence Program, and the ASC NMS Exploration Grants Program.

AUTHOR CONTRIBUTIONS
PJK: Conceptualization, Investigation, Methodology, Resources, Supervision, Visualization, Writing – original draft, Writing – review & editing
HM: Investigation, Visualization, Writing – review & editing
SSL: Methodology, Resources, Writing – review & editing
HOP: Conceptualization, Visualization, Funding acquisition, Methodology, Project administration, Supervision, Writing – original draft, Writing – review & editing

Supplemental Material
Figures S1 – S3
Table S1
Video 1

REFERENCES

1. Etienne-Manneville S. Cdc42--the centre of polarity. J Cell Sci. 2004;117(Pt 8):1291-300. doi: 10.1242/jcs.01115. PubMed PMID: 15020669; PubMed Central PMCID: PMCPMID: 15020669.

2. Park H-O, Bi E. Central roles of small GTPases in the development of cell polarity in yeast and beyond. Microbiol Mol Biol Rev. 2007;71(1):48-96. doi: 10.1128/MMBR.00028-06. PubMed PMID: PMID: 17347519; PubMed Central PMCID: PMCPMC1847380.

3. Reymond N, Im JH, Garg R, Vega FM, Borda d'Agua B, Riou P, et al. Cdc42 promotes transendothelial migration of cancer cells through beta1 integrin. J Cell Biol. 2012;199(4):653-68. doi: 10.1083/jcb.201205169. PubMed PMID: PMID: 23148235; PubMed Central PMCID: PMCPMC3494849.

4. Florian MC, Dorr K, Niebel A, Daria D, Schrezenmeier H, Rojewski M, et al. Cdc42 activity regulates hematopoietic stem cell aging and rejuvenation. Cell Stem Cell. 2012;10(5):520-30. Epub 2012/05/09. doi: 10.1016/j.stem.2012.04.007. PubMed PMID: PMID22560076; PubMed Central PMCID: PMCPMC3348626.

5. Florian MC, Leins H, Gobs M, Han Y, Marka G, Soller K, et al. Inhibition of Cdc42 activity extends lifespan and decreases circulating inflammatory cytokines in aged female C57BL/6 mice. Aging Cell. 2020;19(9):e13208. Epub 2020/08/06. doi: 10.1111/acel.13208. PubMed PMID: 32755011; PubMed Central PMCID: PMCPMC7511875.

6. Nalapareddy K, Hassan A, Sampson LL, Zheng Y, Geiger H. Suppression of elevated Cdc42 activity promotes the regenerative potential of aged intestinal stem cells. iScience. 2021;24(4):102362. Epub 2021/04/20. doi: 10.1016/j.isci.2021.102362. PubMed PMID: 33870147; PubMed Central PMCID: PMCPMC8044426.

7. Kang PJ, Mullner R, Li H, Hansford D, Shen HW, Park H-O. Up-regulation of the Cdc42 GTPase limits the replicative life span of budding yeast. Mol Biol Cell. 2022;33(4):br5. Epub 2022/01/20. doi: 10.1091/mbc.E21-04-0208. PubMed PMID: 35044837; PubMed Central PMCID: PMCPMC9250358.

8. Giebel B. Cell polarity and asymmetric cell division within human hematopoietic stem and progenitor cells. Cells Tissues Organs. 2008;188(1-2):116-26. Epub 2007/12/28. doi: 10.1159/000112842. PubMed PMID: PMID:18160821; PubMed Central PMCID: PMCPMID: 18160821.

9. Florian MC, Klose M, Sacma M, Jablanovic J, Knudson L, Nattamai KJ, et al. Aging alters the epigenetic asymmetry of HSC division. PLoS biology. 2018;16(9):e2003389. Epub 2018/09/21. doi: 10.1371/journal.pbio.2003389. PubMed PMID: 30235201; PubMed Central PMCID: PMCPMC6168157.

10. Wang L, Yang L, Debidda M, Witte D, Zheng Y. Cdc42 GTPase-activating protein deficiency promotes genomic instability and premature aging-like phenotypes. Proceedings of the National Academy of Sciences of the United States of America. 2007;104(4):1248-53. doi: 10.1073/pnas.0609149104. PubMed PMID: PMID: 17227869; PubMed Central PMCID: PMCPMC1783128.

11. Steinkraus KA, Kaeberlein M, Kennedy BK. Replicative aging in yeast: the means to the end. Annual review of cell and developmental biology. 2008;24:29-54. Epub 2008/07/12. doi: 10.1146/annurev.cellbio.23.090506.123509 [doi]. PubMed PMID: 18616424; PubMed Central PMCID: PMCPMC2730916.

12. Campisi J. Aging, cellular senescence, and cancer. Annu Rev Physiol. 2013;75:685-705. Epub 2012/11/13. doi: 10.1146/annurev-physiol-030212-183653. PubMed PMID: 23140366; PubMed Central PMCID: PMCPMC4166529.

13. Ain Q, Schmeer C, Wengerodt D, Witte OW, Kretz A. Extrachromosomal Circular DNA: Current Knowledge and Implications for CNS Aging and Neurodegeneration. Int J Mol Sci. 2020;21(7):2477. Epub 2020/04/08. doi: 10.3390/ijms21072477. PubMed PMID: 32252492; PubMed Central PMCID: PMCPMC7177960.

14. López-Otín C, Blasco MA, Partridge L, Serrano M, Kroemer G. Hallmarks of aging: An expanding universe. Cell. 2023;186(2):243-78. Epub 2023/01/05. doi: 10.1016/j.cell.2022.11.001. PubMed PMID: 36599349; PubMed Central PMCID: PMCPMID: 36599349.

15. Aguilaniu H, Gustafsson L, Rigoulet M, Nystrom T. Asymmetric inheritance of oxidatively damaged proteins during cytokinesis. Science. 2003;299:1751-3. doi: 10.1126/science.1080418. PubMed Central PMCID: PMCPMID: 12610228.

16. Erjavec N, Larsson L, Grantham J, Nyström T. Accelerated aging and failure to segregate damaged proteins in Sir2 mutants can be suppressed by overproducing the protein aggregation-remodeling factor Hsp104p. Genes Dev. 2007;21(19):2410-21. Epub 2007/10/03. doi: 10.1101/gad.439307. PubMed PMID: PMID:17908928; PubMed Central PMCID: PMCPMC1993872.

17. Saarikangas J, Caudron F, Prasad R, Moreno DF, Bolognesi A, Aldea M, et al. Compartmentalization of ER-Bound Chaperone Confines Protein Deposit Formation to the Aging Yeast Cell. Curr Biol. 2017;27(6):773-83. Epub 2017/03/07. doi: 10.1016/j.cub.2017.01.069. PubMed PMID: 28262489.

18. Sinclair DA, Guarente L. Extrachromosomal rDNA circles--a cause of aging in yeast. Cell. 1997;91(7):1033-42. Epub 1998/01/15. doi: 10.1016/s0092-8674(00)80493-6. PubMed PMID: 9428525; PubMed Central PMCID: PMCPMID: 942852.

19. Hotz M, Thayer NH, Hendrickson DG, Schinski EL, Xu J, Gottschling DE. rDNA array length is a major determinant of replicative lifespan in budding yeast. Proceedings of the National Academy of Sciences of the United States of America. 2022;119(15):e2119593119. Epub 2022/04/09. doi: 10.1073/pnas.2119593119. PubMed PMID: 35394872; PubMed Central PMCID: PMCPMC9169770.

20. Hughes AL, Gottschling DE. An early age increase in vacuolar pH limits mitochondrial function and lifespan in yeast. Nature. 2012;492(7428):261-5. Epub 2012/11/23. doi: nature11654 [pii] 10.1038/nature11654 [doi]. PubMed PMID: 23172144; PubMed Central PMCID: PMCPMC3521838.

21. Kaeberlein M, McVey M, Guarente L. The SIR2/3/4 complex and SIR2 alone promote longevity in Saccharomyces cerevisiae by two different mechanisms. Genes Dev. 1999;13(19):2570-80. Epub 1999/10/16. doi: 10.1101/gad.13.19.2570. PubMed PMID: 10521401; PubMed Central PMCID: PMCPMC317077.

22. Kobayashi T, Heck DJ, Nomura M, Horiuchi T. Expansion and contraction of ribosomal DNA repeats in Saccharomyces cerevisiae: requirement of replication fork blocking (Fob1) protein and the role of RNA polymerase I. Genes Dev. 1998;12(24):3821-30. Epub 1998/12/31. doi: 10.1101/gad.12.24.3821. PubMed PMID: 9869636; PubMed Central PMCID: PMCPMC317266.

23. Defossez PA, Prusty R, Kaeberlein M, Lin SJ, Ferrigno P, Silver PA, et al. Elimination of replication block protein Fob1 extends the life span of yeast mother cells. Mol Cell. 1999;3(4):447-55. Epub 1999/05/07. doi: 10.1016/s1097-2765(00)80472-4. PubMed PMID: 10230397.

24. Bi E, Park H-O. Cell polarization and cytokinesis in budding yeast. Genetics. 2012;191(2):347-87. doi: 10.1534/genetics.111.132886. PubMed Central PMCID: PMCPMC3374305.

25. Liu B, Larsson L, Caballero A, Hao X, Oling D, Grantham J, et al. The polarisome is required for segregation and retrograde transport of protein aggregates. Cell. 2010;140(2):257-67. Epub 2010/02/10. doi: 10.1016/j.cell.2009.12.031. PubMed PMID: PMID:20141839; PubMed Central PMCID: PMCPMID: 20141839.

26. Zhou C, Slaughter BD, Unruh JR, Eldakak A, Rubinstein B, Li R. Motility and segregation of Hsp104-associated protein aggregates in budding yeast. Cell. 2011;147(5):1186-96. Epub 2011/11/29. doi: S0092-8674(11)01291-8 [pii] 10.1016/j.cell.2011.11.002 [doi]. PubMed PMID: PMID22118470; PubMed Central PMCID: PMCPMC3237388.

27. Unal E, Kinde B, Amon A. Gametogenesis eliminates age-induced cellular damage and resets life span in yeast. Science. 2011;332(6037):1554-7. Epub 2011/06/28. doi: 10.1126/science.1204349. PubMed PMID: 21700873; PubMed Central PMCID: PMCPMC3923466.

28. Meitinger F, Khmelinskii A, Morlot S, Kurtulmus B, Palani S, Andres-Pons A, et al. A memory system of negative polarity cues prevents replicative aging. Cell. 2014;159(5):1056-69. Epub 2014/11/25. doi: 10.1016/j.cell.2014.10.014. PubMed PMID: 25416945; PubMed Central PMCID: PMCPMID: 25416945.

29. Richman TJ, Sawyer MM, Johnson DI. Saccharomyces cerevisiae Cdc42p localizes to cellular membranes and clusters at sites of polarized growth. Eukaryot Cell. 2002;1(3):458-68. Epub 2002/11/29. PubMed PMID: 12455994; PubMed Central PMCID: PMC118019.

30. Lu MS, Drubin DG. Cdc42 GTPase regulates ESCRTs in nuclear envelope sealing and ER remodeling. J Cell Biol. 2020;219(8):e201910119. Epub 2020/06/20. doi: 10.1083/jcb.201910119. PubMed PMID: 32556066; PubMed Central PMCID: PMCPMC7401818.

31. Kozminski KG, Chen AJ, Rodal AA, Drubin DG. Functions and functional domains of the GTPase Cdc42p. Mol Biol Cell. 2000;11(1):339-54. PubMed PMID: PMID: 10637312; PubMed Central PMCID: PMCPMC14778.

32. Lu MS, Drubin DG. Unexplored Cdc42 functions at the budding yeast nucleus suggested by subcellular localization. Small GTPases. 2022;13(1):255-66. Epub 2021/10/26. doi: 10.1080/21541248.2021.1993714. PubMed PMID: 34689711; PubMed Central PMCID: PMCPMC9707532.

33. Shcheprova Z, Baldi S, Frei SB, Gonnet G, Barral Y. A mechanism for asymmetric segregation of age during yeast budding. Nature. 2008;454(7205):728-34. Epub 2008/07/29. doi: nature07212 [pii] 10.1038/nature07212 [doi]. PubMed PMID: 18660802.

34. Meinema AC, Marzelliusardottir A, Mirkovic M, Aspert T, Lee SS, Charvin G, et al. DNA circles promote yeast ageing in part through stimulating the reorganization of nuclear pore complexes. eLife. 2022;11:e71196. Epub 2022/04/05. doi: 10.7554/eLife.71196. PubMed PMID: 35373738; PubMed Central PMCID: PMCPMC9020822.

35. Li Y, Jin M, O'Laughlin R, Bittihn P, Tsimring LS, Pillus L, et al. Multigenerational silencing dynamics control cell aging. Proceedings of the National Academy of Sciences of the United States of America. 2017;114(42):11253-8. Epub 2017/10/27. doi: 10.1073/pnas.1703379114. PubMed PMID: 29073021; PubMed Central PMCID: PMCPMC5651738.

36. Li Y, Jiang Y, Paxman J, O'Laughlin R, Klepin S, Zhu Y, et al. A programmable fate decision landscape underlies single-cell aging in yeast. Science. 2020;369(6501):325-9. Epub 2020/07/18. doi: 10.1126/science.aax9552. PubMed PMID: 32675375; PubMed Central PMCID: PMCPMC7437498.

37. Lee SS, Avalos Vizcarra I, Huberts DH, Lee LP, Heinemann M. Whole lifespan microscopic observation of budding yeast aging through a microfluidic dissection platform. Proceedings of the National Academy of Sciences of the United States of America. 2012;109(13):4916-20. Epub 2012/03/17. doi: 1113505109 [pii] 10.1073/pnas.1113505109 [doi]. PubMed PMID: 22421136; PubMed Central PMCID: PMC3324001.

38. Xie Z, Zhang Y, Zou K, Brandman O, Luo C, Ouyang Q, et al. Molecular phenotyping of aging in single yeast cells using a novel microfluidic device. Aging Cell. 2012;11(4):599-606. Epub 2012/04/14. doi: 10.1111/j.1474-9726.2012.00821.x [doi]. PubMed PMID: PMID: 22498653; PubMed Central PMCID: PMCPMC3970974.

39. Jo MC, Liu W, Gu L, Dang W, Qin L. High-throughput analysis of yeast replicative aging using a microfluidic system. Proceedings of the National Academy of Sciences of the United States of America. 2015;112(30):9364-9. Epub 2015/07/15. doi: 10.1073/pnas.1510328112. PubMed PMID: 26170317; PubMed Central PMCID: PMCPMC4522780.

40. Moreno DF, Jenkins K, Morlot S, Charvin G, Csikasz-Nagy A, Aldea M. Proteostasis collapse, a hallmark of aging, hinders the chaperone-Start network and arrests cells in G1. eLife. 2019;8. Epub 2019/09/14. doi: 10.7554/eLife.48240. PubMed PMID: 31518229; PubMed Central PMCID: PMCPMC6744273.

41. Liu B, Larsson L, Franssens V, Hao X, Hill SM, Andersson V, et al. Segregation of protein aggregates involves actin and the polarity machinery. Cell. 2011;147(5):959-61. Epub 2011/11/29. doi: 10.1016/j.cell.2011.11.018. PubMed PMID: PMID:22118450; PubMed Central PMCID: PMCPMID: 22118450.

42. Bendezu FO, Vincenzetti V, Vavylonis D, Wyss R, Vogel H, Martin SG. Spontaneous Cdc42 polarization independent of GDI-mediated extraction and actin-based trafficking. PLoS biology. 2015;13(4):e1002097. Epub 2015/04/04. doi: 10.1371/journal.pbio.1002097. PubMed PMID: 25837586; PubMed Central PMCID: PMCPMC4383620.

43. Kang PJ, Miller KE, Guegueniat J, Beven L, Park H-O. The shared role of the Rsr1 GTPase and Gic1/Gic2 in Cdc42 polarization. Mol Biol Cell. 2018;29(20):2359-69. Epub 2018 Aug 9. doi: 10.1091/mbc.E18-02-0145. PubMed PMID: 30091649; PubMed Central PMCID: PMCPMC6233053.

44. Caplan AJ, Tsai J, Casey PJ, Douglas MG. Farnesylation of YDJ1p is required for function at elevated growth temperatures in Saccharomyces cerevisiae. J Biol Chem. 1992;267:18890-5.

45. Ast T, Cohen G, Schuldiner M. A network of cytosolic factors targets SRP-independent proteins to the endoplasmic reticulum. Cell. 2013;152(5):1134-45. Epub 2013/03/05. doi: 10.1016/j.cell.2013.02.003. PubMed PMID: 23452858.

46. Atencio DP, Yaffe MP. MAS5, a yeast homolog of DnaJ involved in mitochondrial protein import. Mol Cell Biol. 1992;12(1):283-91. Epub 1992/01/01. doi: 10.1128/mcb.12.1.283-291.1992. PubMed PMID: 1729605; PubMed Central PMCID: PMCPMC364104.

47. Hildebrandt ER, Cheng M, Zhao P, Kim JH, Wells L, Schmidt WK. A shunt pathway limits the CaaX processing of Hsp40 Ydj1p and regulates Ydj1p-dependent phenotypes. eLife. 2016;5:e15899. doi: 10.7554/eLife.15899.

48. Katoh Y, Nozaki S, Hartanto D, Miyano R, Nakayama K. Architectures of multisubunit complexes revealed by a visible immunoprecipitation assay using fluorescent fusion proteins. J Cell Sci. 2015;128(12):2351-62. Epub 2015/05/13. doi: 10.1242/jcs.168740. PubMed PMID: 25964651.

49. Rothbauer U, Zolghadr K, Muyldermans S, Schepers A, Cardoso MC, Leonhardt H. A versatile nanotrap for biochemical and functional studies with fluorescent fusion proteins. Mol Cell Proteomics. 2008;7(2):282-9. Epub 2007/10/24. doi: M700342-MCP200 [pii] 10.1074/mcp.M700342-MCP200 [doi]. PubMed PMID: 17951627.

50. Kampinga HH, Craig EA. The HSP70 chaperone machinery: J proteins as drivers of functional specificity. Nat Rev Mol Cell Biol. 2010;11(8):579-92. Epub 2010/07/24. doi: 10.1038/nrm2941. PubMed PMID: 20651708; PubMed Central PMCID: PMCPMC3003299.

51. Mandal AK, Nillegoda NB, Chen JA, Caplan AJ. Ydj1 protects nascent protein kinases from degradation and controls the rate of their maturation. Mol Cell Biol. 2008;28(13):4434-44. Epub 2008/04/30. doi: 10.1128/mcb.00543-08. PubMed PMID: 18443039; PubMed Central PMCID: PMCPMC2447146.

52. Flom GA, Lemieszek M, Fortunato EA, Johnson JL. Farnesylation of Ydj1 is required for in vivo interaction with Hsp90 client proteins. Mol Biol Cell. 2008;19(12):5249-58. Epub 2008/10/03. doi: 10.1091/mbc.e08-04-0435. PubMed PMID: 18829866; PubMed Central PMCID: PMCPMC2592663.

53. González B, Aldea M, Cullen PJ. Chaperone-Dependent Degradation of Cdc42 Promotes Cell Polarity and Shields the Protein from Aggregation. Mol Cell Biol. 2023;43(5):200-22. Epub 2023/04/28. doi: 10.1080/10985549.2023.2198171. PubMed PMID: 37114947; PubMed Central PMCID: PMCPMC10184603.

54. González B, Cullen PJ. Regulation of Cdc42 protein turnover modulates the filamentous growth MAPK pathway. J Cell Biol. 2022;221(12). Epub 2022/11/10. doi: 10.1083/jcb.202112100. PubMed PMID: 36350310; PubMed Central PMCID: PMCPMC9811999.

55. Thayer NH, Leverich CK, Fitzgibbon MP, Nelson ZW, Henderson KA, Gafken PR, et al. Identification of long-lived proteins retained in cells undergoing repeated asymmetric divisions. Proceedings of the National Academy of Sciences of the United States of America. 2014;111:14019-26. Epub 2014/09/18. doi: 1416079111 [pii] 10.1073/pnas.1416079111 [doi]. PubMed PMID: 25228775.

56. Yang J, McCormick MA, Zheng J, Xie Z, Tsuchiya M, Tsuchiyama S, et al. Systematic analysis of asymmetric partitioning of yeast proteome between mother and daughter cells reveals "aging factors" and mechanism of lifespan asymmetry. Proceedings of the National Academy of Sciences of the United States of America. 2015;112(38):11977-82. Epub 2015/09/10. doi: 10.1073/pnas.1506054112. PubMed PMID: 26351681; PubMed Central PMCID: PMCPMC4586869.

57. Sugiyama S, Tanaka M. Distinct segregation patterns of yeast cell-peripheral proteins uncovered by a method for protein segregatome analysis. Proc Natl Acad Sci USA. 2019;116:8909-18. PubMed PMID: PMID: 30975753; PubMed Central PMCID: PMCPMC6500170.

58. Guthrie C, Fink GR. Guide to Yeast Genetics and Molecular Biology. San Diego: Academic Press; 1991. 933 p.

59. Summers DW, Douglas PM, Ren HY, Cyr DM. The type I Hsp40 Ydj1 utilizes a farnesyl moiety and zinc finger-like region to suppress prion toxicity. The Journal of biological chemistry. 2009;284(6):3628-39. Epub 2008/12/06. doi: 10.1074/jbc.M807369200. PubMed PMID: 19056735; PubMed Central PMCID: PMCPMC2635041.

60. Miller KE, Lo WC, Chou CS, Park H-O. Temporal regulation of cell polarity via the interaction of the Ras GTPase Rsr1 and the scaffold protein Bem1. Mol Biol Cell. 2019;30(20):2543-57. Epub 20190814. doi: 10.1091/mbc.E19-02-0106. PubMed PMID: 31411940; PubMed Central PMCID: PMCPMC6740199.

61. Kennedy BK, Austriaco NR, Jr., Guarente L. Daughter cells of Saccharomyces cerevisiae from old mothers display a reduced life span. J Cell Biol. 1994;127(6 Pt 2):1985-93. Epub 1994/12/01. doi: 10.1083/jcb.127.6.1985. PubMed PMID: PMID:7806576; PubMed Central PMCID: PMCPMC2120297.

62. Cox JS, Chapman RE, Walter P. The unfolded protein response coordinates the production of endoplasmic reticulum protein and endoplasmic reticulum membrane. Mol Biol Cell. 1997;8(9):1805-14. Epub 1997/10/06. doi: 10.1091/mbc.8.9.1805. PubMed PMID: 9307975; PubMed Central PMCID: PMCPMC305738.

FIGURE LEGENDS

Fig. 1. Microfluidic imaging of WT cells shows elevation of Cdc42 levels during aging

A. Two representative WT cells expressing Cdc42-mCherry^{SW} are shown at selected time points (hr: min) from the initial loading, together with their ages. White arrowheads mark cells during or shortly after cytokinesis, when Cdc42 levels were quantified as shown in **Fig. 1B** and **Fig. 3, B** & **C**. Black or red arrowheads indicate the same cell at a different cell cycle stage or death, respectively. Scale bar = 3 μm. See Video 1.

B. Mean intensity of Cdc42-mCherry^{SW} fluorescence in each large-budded cell (see legend in **A**) at young (ages 1 to 3) versus old ages (the last three divisions). Each circle on the graphs represents the average intensity from 3 divisions of individual cells (n = 42). The *p*-values were obtained from paired t-tests: ***, $p < 0.001$.

C. Cdc42 proteins in WT and *cdc42-108* strains were detected by immunoblotting using a monoclonal anti-Cdc42 antibody. Numbers (bottom) represent Cdc42 levels normalized with the loading control, α-tubulin.

D. The percentage (mean ± SEM) of cell survival at each age of WT and *cdc42-108* mutant. Numbers in parentheses indicate the median lifespan. The *p*-value is obtained from the Log-Rank (Mantel-Cox) test: *, $p = 0.031$; n = 116 for each strain.

Fig. 2. Cdc42 upregulation limits lifespan independently of rDNA desilencing

A. Representative cell morphology during yeast aging observed by microfluidic imaging: (a) a cell dying in the unbudded state, (b) a cell producing round buds (marked with yellow arrows) until death, and (c) a cell forming elongated buds (marked with blue arrows) during aging. Ages and relevant time points are marked with white and black letters. Scale bar = 3 μm. Below, the terminal cell shapes of WT1 (BY4741) and two isogenic strains, WT2 (HPY210) and $CDC42_{OV}$ (HPY3721), are quantified (n = 40–60 for each strain).

B. Cell survival curves for *fob1Δ* and *fob1Δ cdc42-108* mutants. Refer to the legend in **Fig. 1D**. The *p*-value is from the Log-rank test: ****, $p < 0.0001$; n = 114 for *fob1Δ,* and n = 134 for *fob1Δ cdc42-108*.

Fig. 3. Asymmetric distribution of Cdc42 during cell divisions via endomembrane association

A. Cdc42-mCherry^{SW} levels in each pair of young or old mothers and their daughters in M–cytokinesis (see legend in **Fig. 1B**). Each circle on the graphs represents the average intensity from 3 divisions of individual cells (n = 42). The *p*-values were obtained from paired t-tests: ****, $p < 0.0001$.

B. Cdc42-mCherry^{SW} levels in mother and daughter pairs at the last division before both cells' death (e.g., Cell 2 in **Fig. 1A**). The *p*-value was obtained from a paired t-test: ns, $p \geq 0.05$.

C. Localization and quantification of Cdc42-ritC-GFP. Scale bar = 3 μm. A scheme (left) highlights the amphipathic helix (blue) from Rit replacing the CaaX motif of WT Cdc42. The graph (right) shows the mean fluorescence intensity of Cdc42-ritC-GFP in the mother and bud compartments from 20 representative cells in M-cytokinesis.

Fig. 4. Farnesylated Ydj1 is involved in asymmetric distribution of Cdc42.

A. Localization of Cdc42-mCherry^{SW} in WT and *ydj1* mutants at 27°C. Arrows mark examples of large-budded cells in which Cdc42 levels were quantified in **B** & **C**. Scale bar = 3 μm.

B. Mean fluorescence intensities of Cdc42-mCherry^{SW} in *ydj1Δ* cells with large buds are compared in the mother (m) and bud (b) compartments: 18 representative cells are plotted on the left. The differences in mean intensity between the mother and bud compartments are plotted for each strain (n = 52 for each strain) and analyzed by a one-way ANOVA ($p < 0.0001$).
C. Global fluorescence intensities of Cdc42-mCherry^{SW} in WT and *ydj1* mutants. Mean fluorescence intensities in the whole cells (including both mother and bud compartments) are shown on the graph (n = 52 for each strain). The *p*-values were obtained from unpaired t-tests: ***, $p < 0.001$; and ****, $p < 0.0001$. An immunoblot shows Cdc42-mCherry^{SW} protein in WT and *ydj1Δ* strains, detected using polyclonal anti-RFP antibodies. Numbers (at the bottom) show Cdc42-mCherry^{SW} levels normalized using the loading control, α-tubulin.
D. Association of Cdc42-mCherry^{SW} with GFP-Ydj1 on the beads from a visible IP assay (see the diagram on the right) using lysates carrying CDC42-mCherry^{SW} and GFP-YDJ1 (top panels) or an untagged YDJ1 (bottom panels) as a control.

LEGENDS FOR SUPPLEMENTAL FIGURES AND VIDEO

Fig. S1. Quantification of Cdc42 levels in growing buds.
Mean pixel intensities of Cdc42-mCherry^{SW} within buds are compared in cells with different bud sizes, as schematically shown in the middle, with images on the right. A split septin ring (labeled with Cdc3-GFP) marks the onset of cytokinesis. Arrows indicate the same bud that develops and gives rise to a daughter cell. A dotted arrow indicates a daughter cell from the previous division before being washed away during microfluidic imaging. *P* values were obtained from Student's t-tests (n = 30 for each stage): ns, $p \geq 0.05$; *, $p < 0.05$; and ***, $p < 0.001$.

Fig. S2. Blot transparency
A. Cdc42 protein in wild-type and *cdc42-108* strains was detected using anti-Cdc42 monoclonal antibody (a), and α-tubulin was detected with anti-α-tubulin monoclonal antibody (b). A minor cross-reacting signal of Cdc42 in (b) was seen because the same secondary antibody solution was used for the control blot after detecting Cdc42 in (a). 12.5% gels were used. See Fig. 1C.
B. Cdc42-mCherrySW and α-tubulin were detected using anti-RFP polyclonal antibodies and anti-α-tubulin monoclonal antibody, respectively. See Fig. 4C.

Fig. S3. Growth phenotype of *ydj1* mutants.
WT strain and *ydj1*Δ and *ydj1*^{C406S} mutants in the isogenic background were grown on YPD plates at 27°C, 30°C, and 37°C.

Video 1. Microfluidic-assisted imaging of WT cells expressing Cdc42-mCherry^{SW}.
Images were captured every 20 min at 27°C using an inverted widefield microscope (TiE, Nikon), and fluorescence images were deconvolved. The video shows frames for 56 hr 20 min of Cell 1, with selected time points shown in **Fig. 1A**. The display rate is 8 frames per sec (fps).

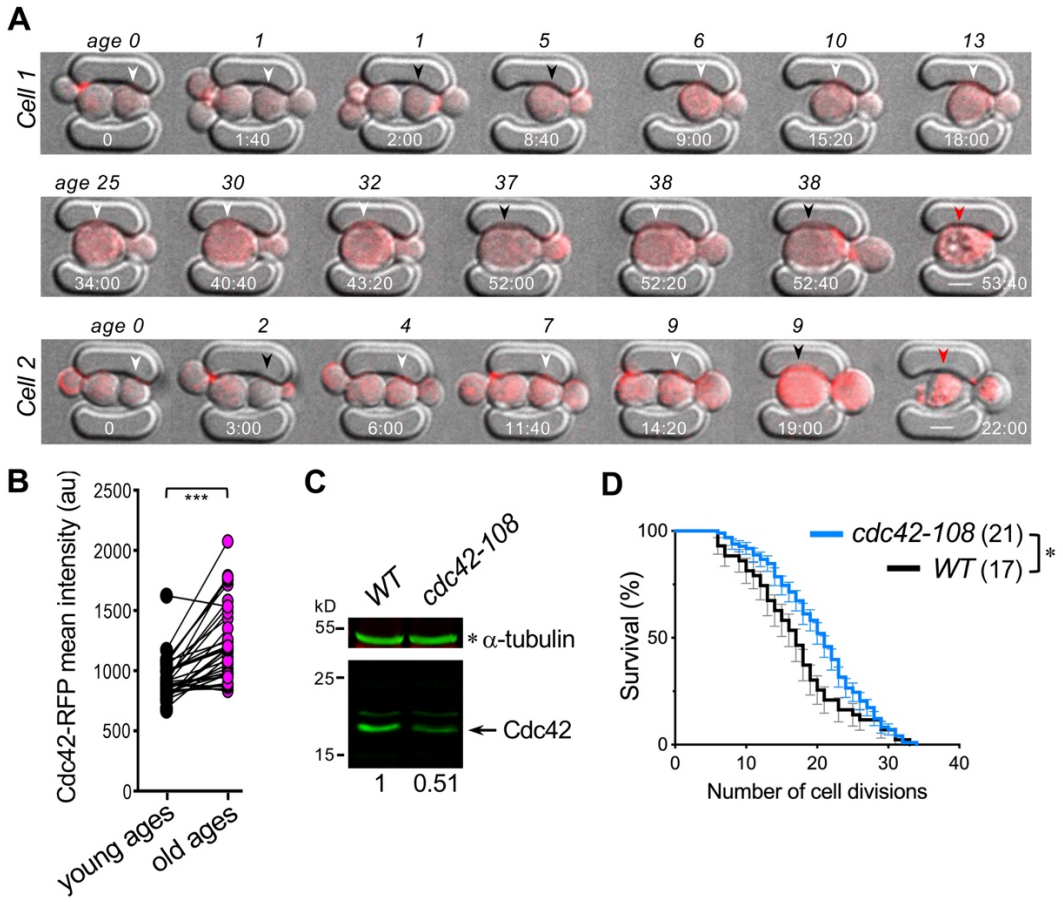

Fig. 1. Microfluidic imaging of WT cells shows elevation of Cdc42 levels during aging

A. Two representative WT cells expressing Cdc42-mCherry^{SW} are shown at selected time points (hr: min) from the initial loading, together with their ages. White arrowheads mark cells during or shortly after cytokinesis, when Cdc42 levels were quantified as shown in Fig. 1B and Fig. 3, B & C. Black or red arrowheads indicate the same cell at a different cell cycle stage or death, respectively. Scale bar = 3 µm. See Video 1.

B. Mean intensity of Cdc42-mCherry^{SW} fluorescence in each large-budded cell (see legend in A) at young (ages 1 to 3) versus old ages (the last three divisions). Each circle on the graphs represents the average intensity from 3 divisions of individual cells (n = 42). The *p*-values were obtained from paired t-tests: ***, $p < 0.001$.

C. Cdc42 proteins in WT and *cdc42-108* strains were detected by immunoblotting using a monoclonal anti-Cdc42 antibody. Numbers (bottom) represent Cdc42 levels normalized with the loading control, α-tubulin.

D. The percentage (mean ± SEM) of cell survival at each age of WT and *cdc42-108* mutant. Numbers in parentheses indicate the median lifespan. The *p*-value is obtained from the Log-Rank (Mantel-Cox) test: *, $p = 0.031$; n = 116 for each strain.

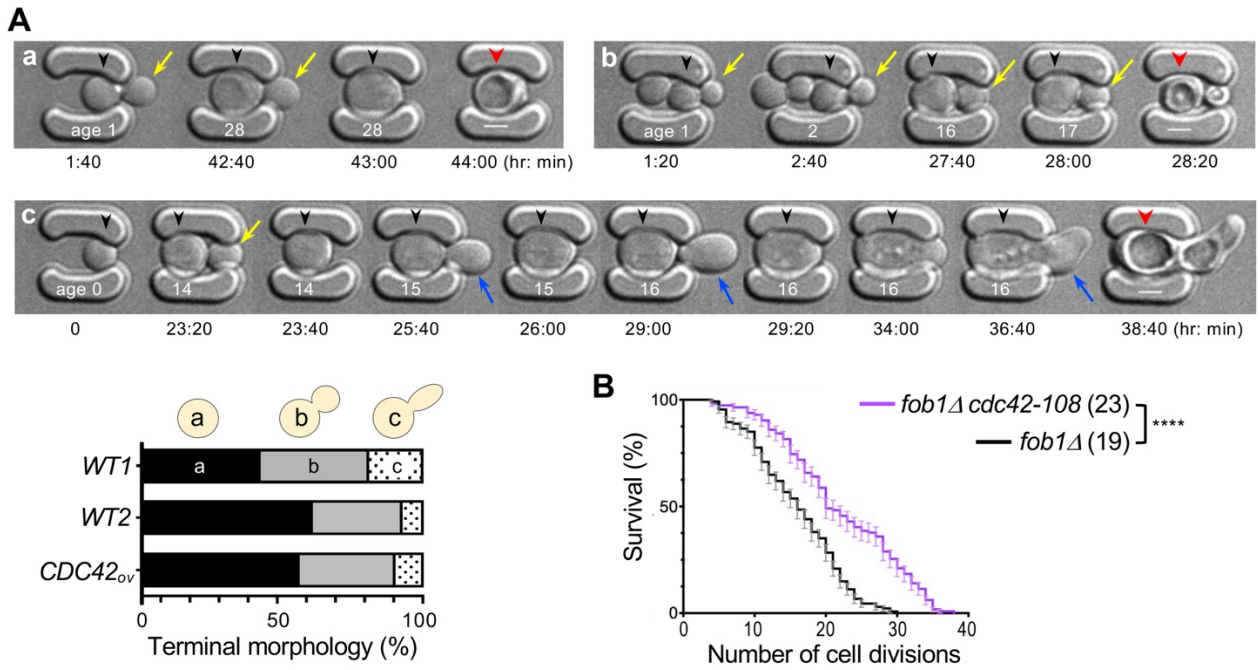

Fig. 2. Cdc42 upregulation limits lifespan independently of rDNA desilencing

A. Representative cell morphology during yeast aging observed by microfluidic imaging: (a) a cell dying in the unbudded state, (b) a cell producing round buds (marked with yellow arrows) until death, and (c) a cell forming elongated buds (marked with blue arrows) during aging. Ages and relevant time points are marked with white and black letters. Scale bar = 3 μm. Below, the terminal cell shapes of WT1 (BY4741) and two isogenic strains, WT2 (HPY210) and *CDC42*$_{OV}$ (HPY3721), are quantified (n = 40–60 for each strain).

B. Cell survival curves for *fob1Δ* and *fob1Δ cdc42-108* mutants. Refer to the legend in Fig. 1D. The *p*-value is from the Log-rank test: ****, $p < 0.0001$; n = 114 for *fob1Δ,* and n = 134 for *fob1Δ cdc42-108*.

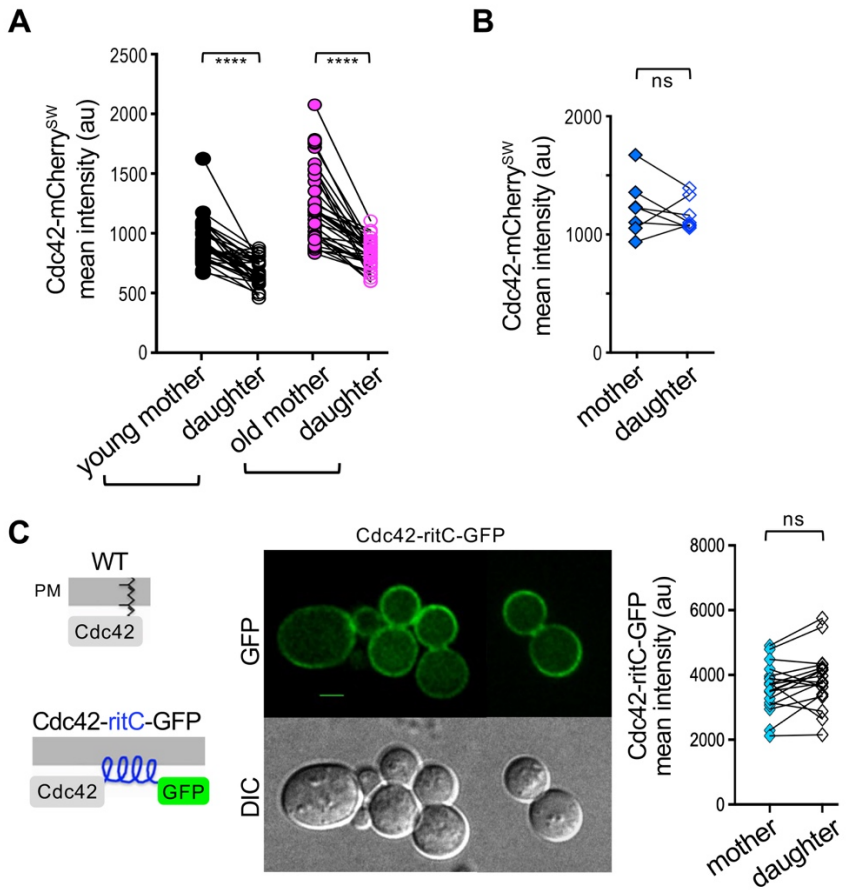

Fig. 3. Asymmetric distribution of Cdc42 during cell divisions via endomembrane association

A. Cdc42-mCherry^{SW} levels in each pair of young or old mothers and their daughters in M–cytokinesis (see legend in **Fig. 1B**). Each circle on the graphs represents the average intensity from 3 divisions of individual cells (n = 42). The *p*-values were obtained from paired t-tests: ****, $p < 0.0001$.

B. Cdc42-mCherry^{SW} levels in mother and daughter pairs at the last division before both cells' death (e.g., Cell 2 in **Fig. 1A**). The *p*-value was obtained from a paired t-test: ns, $p \geq 0.05$.

C. Localization and quantification of Cdc42-ritC-GFP. Scale bar = 3 µm. A scheme (left) highlights the amphipathic helix (blue) from Rit replacing the CaaX motif of WT Cdc42. The graph (right) shows the mean fluorescence intensity of Cdc42-ritC-GFP in the mother and bud compartments from 20 representative cells in M-cytokinesis.

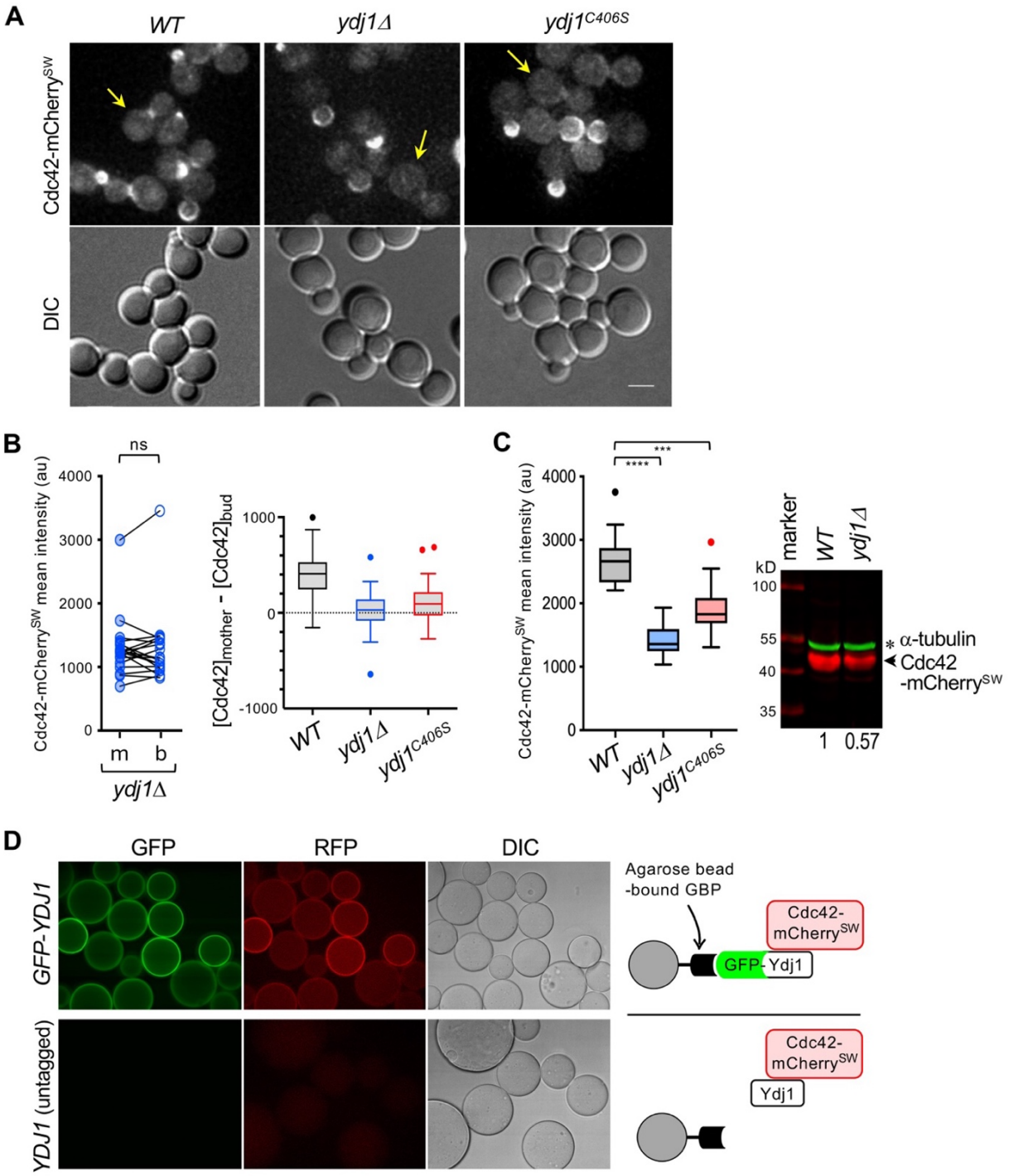

Fig. 4. Farnesylated Ydj1 is involved in asymmetric distribution of Cdc42.

A. Localization of Cdc42-mCherry^{SW} in WT and *ydj1* mutants at 27°C. Arrows mark examples of large-budded cells in which Cdc42 levels were quantified in B & C. Scale bar = 3 µm.

B. Mean fluorescence intensities of Cdc42-mCherry^{SW} in *ydj1Δ* cells with large buds are compared in the mother (m) and bud (b) compartments: 18 representative cells are plotted on the left. The differences in mean intensity between the mother and bud compartments are plotted for each strain (n = 52 for each strain) and analyzed by a one-way ANOVA ($p < 0.0001$).

C. Global fluorescence intensities of Cdc42-mCherry^{SW} in WT and *ydj1* mutants. Mean fluorescence intensities in the whole cells (including both mother and bud compartments) are shown on the graph (n = 52 for each strain). The *p*-values were obtained from unpaired t-tests: ***, $p < 0.001$; and ****, $p < 0.0001$. An immunoblot shows Cdc42-mCherry^{SW} protein in WT and *ydj1Δ* strains, detected using polyclonal anti-RFP antibodies. Numbers (at the bottom) show Cdc42-mCherry^{SW} levels normalized using the loading control, α-tubulin.

D. Association of Cdc42-mCherry^{SW} with GFP-Ydj1 on the beads from a visible IP assay (see the diagram on the right) using lysates carrying CDC42-mCherry^{SW} and GFP-YDJ1 (top panels) or an untagged YDJ1 (bottom panels) as a control.

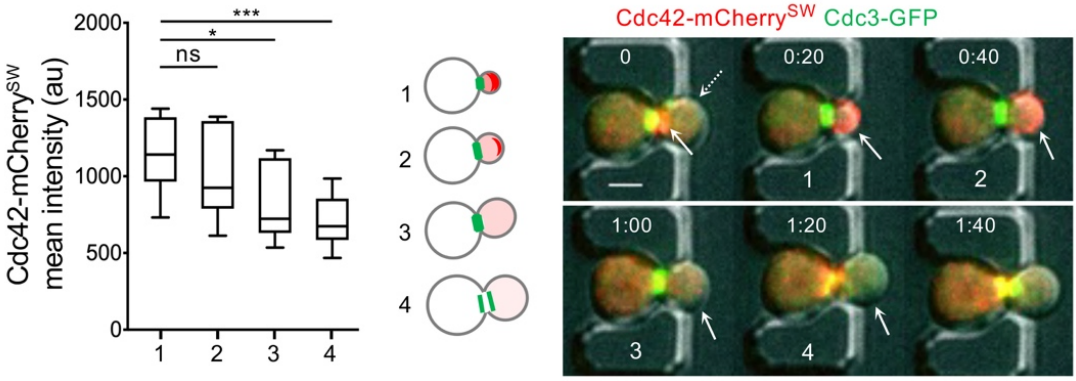

Fig. S1. Quantification of Cdc42 levels in growing buds.

Mean pixel intensities of Cdc42-mCherry^{SW} within buds are compared in cells with different bud sizes, as schematically shown in the middle, with images on the right. A split septin ring (labeled with Cdc3-GFP) marks the onset of cytokinesis. Arrows indicate the same bud that develops and gives rise to a daughter cell. A dotted arrow indicates a daughter cell from the previous division before being washed away during microfluidic imaging. *P* values were obtained from Student's t-tests (n = 30 for each stage): ns, $p \geq 0.05$; *, $p < 0.05$; and ***, $p < 0.001$.

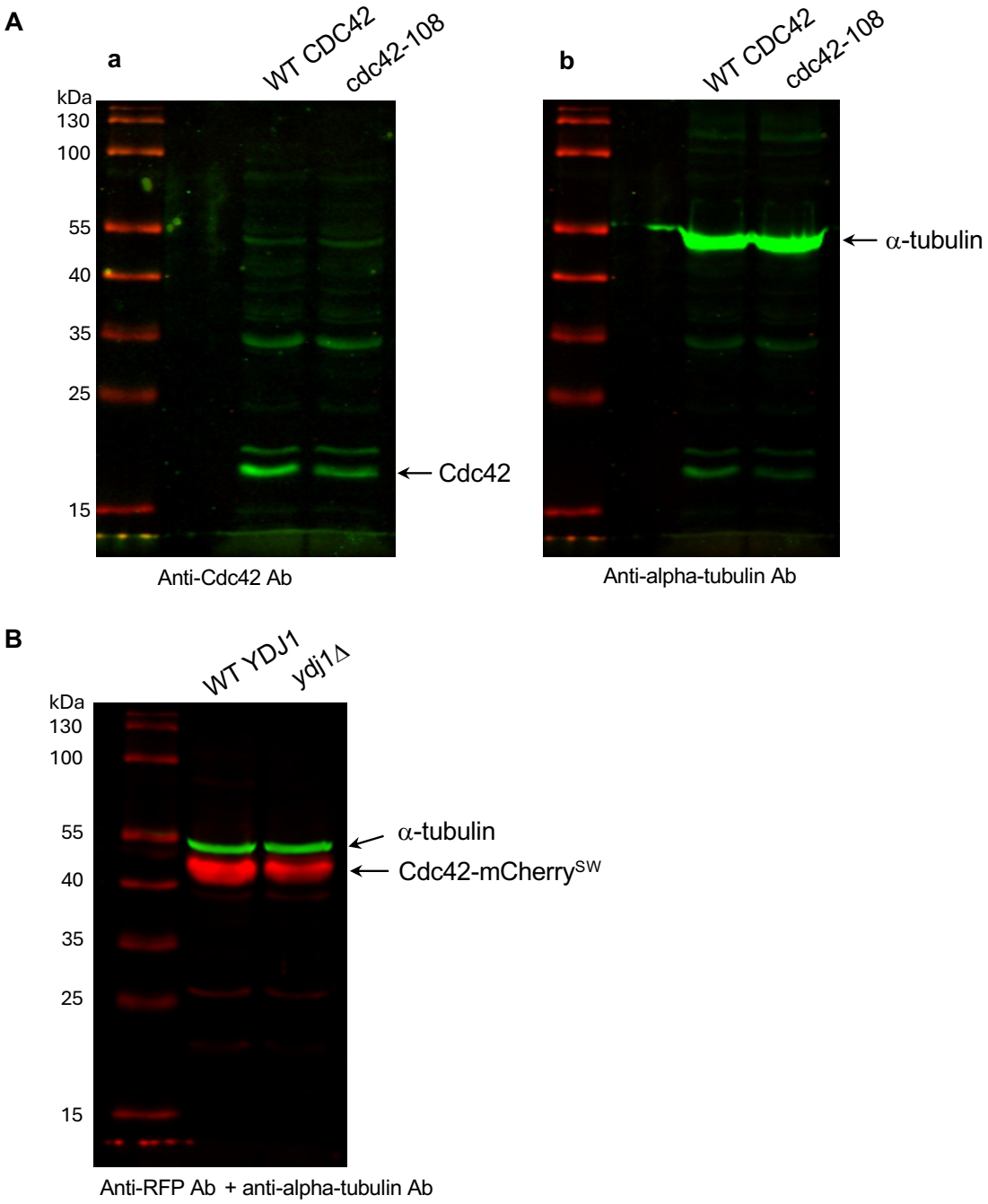

Fig. S2. Blot transparency

A. Cdc42 protein in wild-type and *cdc42-108* strains was detected using anti-Cdc42 monoclonal antibody (a), and α-tubulin was detected with anti-α-tubulin monoclonal antibody (b). A minor cross-reacting signal of Cdc42 in (b) was seen because the same secondary antibody solution was used for the control blot after detecting Cdc42 in (a). 12.5% gels were used. See Fig. 1C.

B. Cdc42-mCherrySW and α-tubulin were detected using anti-RFP polyclonal antibodies and anti-α-tubulin monoclonal antibody, respectively. See Fig. 4C.

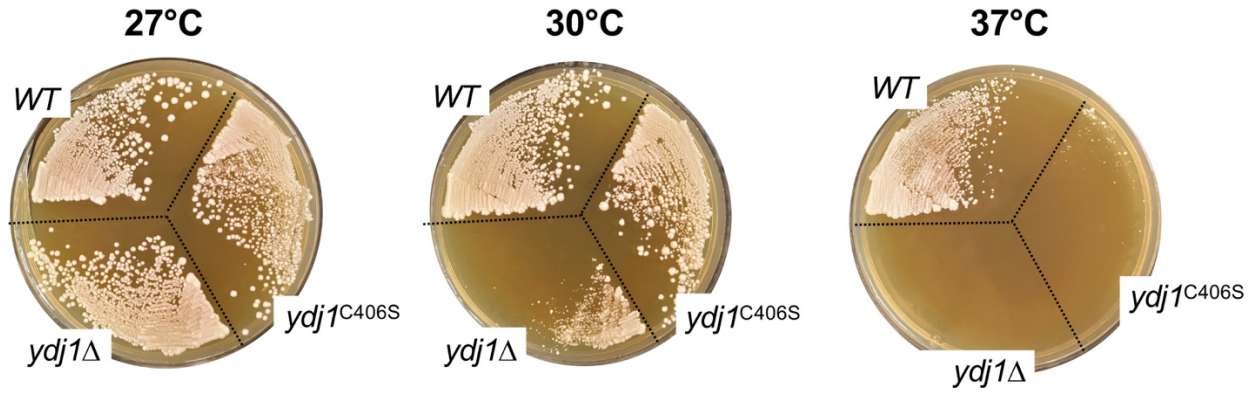

Fig. S3. Growth phenotype of *ydj1* mutants

WT strain and *ydj1*Δ and *ydj1*^{C406S} mutants in the isogenic background were grown on YPD plates at 27°C, 30°C, and 37°C.

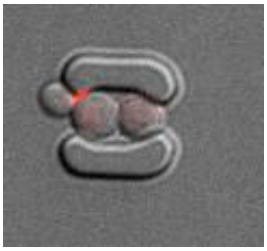

Video 1. Microfluidic-assisted imaging of WT cells expressing Cdc42-mCherry^{SW}.

Images were captured every 20 min at 27°C using an inverted widefield microscope (TiE, Nikon), and fluorescence images were deconvolved. The video shows frames for 56 hr 20 min of Cell 1, with selected time points shown in **Fig. 1A**. The display rate is 8 frames per sec (fps)**.**